Tunable coupler for superconducting Xmon qubits: Perturbative nonlinear model

Michael R. Geller,[1,*] Emmanuel Donate,[1] Yu Chen,[2,†] Michael T. Fang,[2] Nelson Leung,[2] Charles Neill,[2] Pedram Roushan,[2,†] and John M. Martinis[2,3]

[1]*Department of Physics and Astronomy, University of Georgia, Athens, Georgia 30602, USA*

[2]*Department of Physics, University of California, Santa Barbara, California 93106, USA*

[3]*Google Inc., Santa Barbara, California 93117, USA*

(Received 13 May 2014; published 17 July 2015)

We study a recently demonstrated design for a high-performance tunable coupler suitable for superconducting Xmon and planar transmon qubits [Y. Chen *et al.*, Phys. Rev. Lett. **113**, 220502 (2014)]. The coupler circuit uses a single flux-biased Josephson junction and acts as a tunable current divider. We calculate the effective qubit-qubit interaction Hamiltonian by treating the nonlinearity of the qubit and coupler junctions perturbatively. We find that the qubit nonlinearity has two principal effects: The first is to suppress the magnitude of the transverse $\sigma^x \otimes \sigma^x$ coupling from that obtained in the harmonic approximation by about 15%, assuming typical qubit parameters. The second is to induce a small diagonal $\sigma^z \otimes \sigma^z$ coupling. The effects of the coupler junction nonlinearity are negligible in the parameter regime considered. The approach used here can be applied to other complex nonlinear circuits arising in the design of superconducting hardware for quantum information processing.

DOI: 10.1103/PhysRevA.92.012320 PACS number(s): 03.67.Lx, 85.25.Cp

I. INTRODUCTION

The development of a fully planar transmon-type [1] superconducting qubit, which combines high coherence with several other features desirable for logic gate implementation and scalability, could make a quantum computer based on quantum integrated circuits possible in the near future [2]. These Xmon qubits can be directly wired together (or to a resonator bus) with fixed capacitors [3], but the resulting couplings are always present and degrade gate performance. A simple tunable coupler option is therefore desirable. Tunable coupling is also often desirable for quantum simulation applications [4–6] as well.

A wide variety of tunable coupler designs for superconducting circuits have been considered previously [4,7–25]. However, most of these designs are intended for flux qubits, and high-performance applications have yet to be realized due to the challenges of implementing tunable coupling while maintaining qubit coherence. Furthermore, large crosstalk errors arise when there is a dc path connecting the qubit and coupler junctions.

The coupler we discuss in this work is suitable for Xmon [2] and planar transmon [1] qubits, which have no trapped flux, and the design is experimentally practical. In contrast to previous couplers, the design discussed here inductively couples transmon qubits at their low-voltage nodes. This is desirable because it reduces the energy stored in the coupler junction, diminishing its nonlinear behavior. In fact, we find that the effects of coupler junction nonlinearity are negligible in this design. Furthermore, crosstalk errors are minimized by eliminating the dc coupling between the qubits. Most importantly, the design introduces tunability without compromising high coherence. Tunably coupled Xmon's based on this design, which are called gmon qubits, have been demonstrated recently [26]. The analysis of Ref. [26] is based on a harmonic circuit model, and the important effects of nonlinearity have yet to be considered. In this work we study this coupler design theoretically, focusing on the effects of the circuit nonlinearity.

Nonlinearity can in principal affect both the form and strength of the qubit-qubit interaction. Because the coupling here is purely inductive, the interaction Hamiltonian is proportional to $\sigma^x \otimes \sigma^x$ and $\sigma^z \otimes \sigma^z$. In this work we show that the qubit anharmonicity suppresses the magnitude of the transverse $\sigma^x \otimes \sigma^x$ coupling from that obtained in the harmonic approximation, as well as induces a small diagonal $\sigma^z \otimes \sigma^z$ coupling.

The organization of this paper is as follows. In Sec. II we introduce the coupler circuit and derive a simple formula for the tunable coupling in the weak coupling and harmonic limit. In Sec. III we construct the Hamiltonian for the nonlinear circuit and in Sec. IV calculate the transverse coupling numerically by exact diagonalization. In Sec. V we calculate the $\sigma^x \otimes \sigma^x$ coupling for the linearized model beyond weak coupling and study the nonlinearity perturbatively. In Sec. VI we calculate the diagonal $\sigma^z \otimes \sigma^z$ coupling, both analytically and numerically. In Sec. VII we give our conclusions and also comment on the choice of possible circuit parameter values and the behavior of the coupler as these values are varied. Two appendixes contain details of the calculations that are not essential for the general reader.

II. HARMONIC LIMIT

The coupler circuit is shown in Fig. 1. We begin by briefly discussing the circuit in the harmonic approximation. Josephson junctions (crosses) are characterized by their zero-bias linear inductances L_j and L_T. In particular, $L_T = \Phi_0/2\pi I_c$, where $\Phi_0 \equiv h/2e$ and I_c is the critical current of the coupler junction. A magnetic flux bias Φ_{ext} is used to tune the coupler junction's effective linear inductance to $L_{eff} = L_T/\cos\delta$, where δ is the dc phase difference across the coupler. The relation between δ and Φ_{ext} follows from writing the total magnetic flux $\Phi \equiv \oint_\Gamma \mathbf{A}\cdot d\mathbf{l} = (\delta/2\pi)\Phi_0$ in the coupler loop

*mgeller@uga.edu

†Present address: Google Inc., Santa Barbara, California 93117, USA.

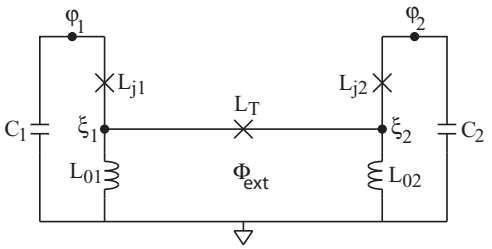

FIG. 1. Coupler circuit schematic. The φ_i and ξ_i are node flux variables, and $\Phi_{\rm ext}$ is an external magnetic flux bias. There are four active nodes (black dots) in this circuit. The Josephson junctions labeled $L_{\rm j}$ are each double junctions threaded by additional fluxes (not shown) that tune the qubit frequencies.

Γ as $\Phi = \Phi_{\rm ext} - L_{\rm loop} I_{\rm c} \sin\delta$, where $L_{\rm loop} = L_{01} + L_{02}$. Here $I_{\rm c}\sin\delta$ is the induced supercurrent. This leads to

$$\delta + \left(\frac{L_{01}+L_{02}}{L_{\rm T}}\right)\sin\delta = \phi_{\rm ext}, \tag{1}$$

where $\phi_{\rm ext} \equiv 2\pi\,\Phi_{\rm ext}/\Phi_0$.

When $L_{\rm eff} \to \infty$, no ac current flows through the coupler and the circuit describes two uncoupled qubits. This occurs when

$$\delta \bmod 2\pi = \left(\frac{\pi}{2}, \frac{3\pi}{2}\right). \tag{2}$$

Then (1) shows that the coupling vanishes when

$$\phi_{\rm ext} \bmod 2\pi = \left(\frac{\pi}{2} + \frac{L_{01}+L_{02}}{L_{\rm T}}, \frac{3\pi}{2} - \frac{L_{01}+L_{02}}{L_{\rm T}}\right). \tag{3}$$

In the weakly coupled limit the effective coupling strength—half the splitting between the symmetric and antisymmetric eigenstates—is approximately [26]

$$g = -\frac{L_0^2\cos\delta}{2(L_{\rm j}+L_0)(L_{\rm T}+2L_0\cos\delta)}\,\omega_{\rm q}, \tag{4}$$

where $\omega_{\rm q}$ is the qubit frequency. This is derived in Appendix A. In (4) we have assumed identical qubits in resonance. The expression (4) is valid in the weak coupling limit and, in addition, does not account for qubit and coupler anharmonicity (beyond the flux-dependence of the linear inductance $L_{\rm eff}$).

In Table I we provide an example of possible system parameter values. The approximate coupling function (4) for these parameters is shown in Fig. 2. Here $\delta(\phi_{\rm ext})$ is obtained from (1). With these parameter values the coupling vanishes at $\phi_{\rm ext} \bmod 2\pi = (0.598\pi, 1.402\pi)$.

In the remainder of this paper we calculate the transverse $\sigma^x \otimes \sigma^x$ coupling g, going beyond the approximations leading to (4), and we also compute the diagonal $\sigma^z \otimes \sigma^z$ coupling.

TABLE I. Example values of circuit parameters.

quantity	value
C_1, C_2	91 fF
$L_{\rm j1}, L_{\rm j2}$	8.6 nH
L_{01}, L_{02}	200 pH
$L_{\rm T}$	1.3 nH

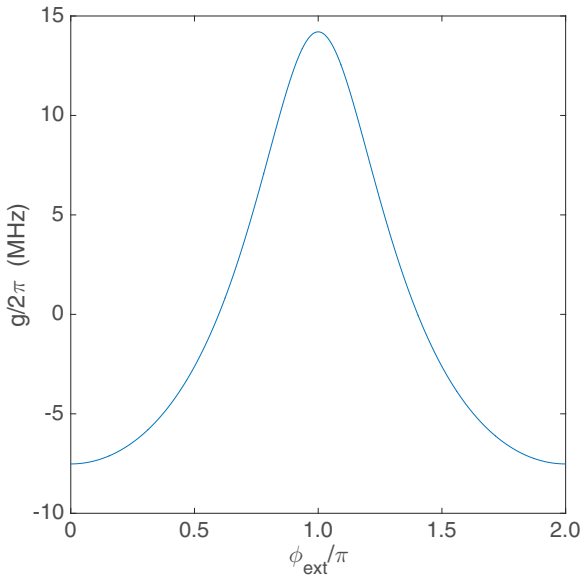

FIG. 2. (Color online) Coupling strength in the weak coupling limit (4), for system parameters given in Table I.

III. NONLINEAR CIRCUIT MODEL

The state of the circuit in Fig. 1 is described by four coordinates. However the ξ_1 and ξ_2 nodes have negligible capacitance to ground, and therefore are massless degrees of freedom that remain in their instantaneous ground states. They will be eliminated from the problem in the analysis below. The complete Lagrangian for the circuit of Fig. 1 is

$$L = \sum_{i=1,2}\left(\frac{\Phi_0}{2\pi}\right)^2\frac{C_i}{2}\dot{\varphi}_i^2 - U, \tag{5}$$

where

$$U = \sum_{i=1,2}\left\{\left(\frac{\Phi_0}{2\pi}\right)^2\left[\frac{\xi_i^2}{2L_{0i}} - \frac{\cos(\varphi_i-\xi_i)}{L_{ji}}\right]\right\} - \left(\frac{\Phi_0}{2\pi}\right)^2\frac{\cos(\xi_1-\xi_2-\phi_{\rm ext})}{L_{\rm T}}. \tag{6}$$

We begin our analysis by writing the four coordinates as classical equilibrium or dc values that minimize the potential energy (6), plus deviations. Two of the four equilibrium conditions lead to

$$\bar{\varphi}_i = \bar{\xi}_i, \tag{7}$$

where the bar denotes equilibrium values. The remaining two conditions can be written as

$$\frac{\bar{\xi}_1}{L_{01}} = -x \quad \text{and} \quad \frac{\bar{\xi}_2}{L_{02}} = x, \tag{8}$$

where $x \equiv \sin(\bar{\xi}_1 - \bar{\xi}_2 - \phi_{\rm ext})/L_{\rm T}$. This leads to

$$x = -\frac{\sin[(L_{01}+L_{02})\,x + \phi_{\rm ext}]}{L_{\rm T}}. \tag{9}$$

We solve (9) approximately, in the weak coupling limit. To do this we define $y \equiv (L_{01}+L_{02})\,x$, which leads to

$$y = -\frac{L_{01}+L_{02}}{L_{\rm T}}\sin(y+\phi_{\rm ext}). \tag{10}$$

Solving (10) iteratively leads to a solution expressed as a power series in $(L_{01}+L_{02})/L_{\rm T}$. The solution to second order is

$$y = -\frac{L_{01}+L_{02}}{L_{\rm T}}\sin(\phi_{\rm ext}) + \frac{1}{2}\left(\frac{L_{01}+L_{02}}{L_{\rm T}}\right)^2\sin(2\phi_{\rm ext}). \tag{11}$$

Putting everything together we obtain

$$\bar{\varphi}_1 = \bar{\xi}_1 = \frac{L_{01}}{L_{\rm T}}\left(\sin\phi_{\rm ext} - \frac{L_{01}+L_{02}}{2L_{\rm T}}\sin 2\phi_{\rm ext}\right) \tag{12}$$

and

$$\bar{\varphi}_2 = \bar{\xi}_2 = -\frac{L_{02}}{L_{\rm T}}\left(\sin\phi_{\rm ext} - \frac{L_{01}+L_{02}}{2L_{\rm T}}\sin 2\phi_{\rm ext}\right). \tag{13}$$

Finally, we rewrite the circuit Lagrangian (5) and (6) in terms of the equilibrium coordinates. After a change of variables

$$\varphi_i \to \bar{\varphi}_i + \varphi_i, \quad \xi_i \to \bar{\xi}_i + \xi_i, \tag{14}$$

the potential (6) becomes

$$U = \sum_{i=1,2}\left\{\left(\frac{\Phi_0}{2\pi}\right)^2\left[\frac{(\bar{\xi}_i+\xi_i)^2}{2L_{0i}} - \frac{\cos(\varphi_i-\xi_i)}{L_{ji}}\right]\right\} - \left(\frac{\Phi_0}{2\pi}\right)^2\frac{\cos(\xi_1-\xi_2-\delta)}{L_{\rm T}}, \tag{15}$$

where the φ_i and ξ_i variables now denote *deviations* from equilibrium, and

$$\delta \equiv \phi_{\rm ext} + \bar{\xi}_2 - \bar{\xi}_1. \tag{16}$$

The function (16) relates the dc phase difference δ across the coupler junction to the external flux.

Now we are ready to construct the Hamiltonian: The momentum conjugate to φ_i is

$$p_i = \left(\frac{\Phi_0}{2\pi}\right)^2 C_i\,\dot{\varphi}_i. \tag{17}$$

The momenta conjugate to the ξ_i vanish. The complete Hamiltonian for the circuit of Fig. 1 is therefore

$$H = \left(\frac{2\pi}{\Phi_0}\right)^2\sum_i\frac{p_i^2}{2C_i} + U, \tag{18}$$

where U is given in (15).

IV. EXACT DIAGONALIZATION CALCULATION OF THE COUPLING

To validate our perturbative nonlinear analysis it is useful to study the nonlinear model numerically. In Fig. 3 we plot the splitting between the symmetric and antisymmetric eigenstates—equal to twice the magnitude of the transverse component of the effective coupling strength—for the full nonlinear model (15), assuming the circuit parameters given in Table I. To obtain these results we use a two-dimensional grid in the coordinates φ_1 and φ_2, and the basis

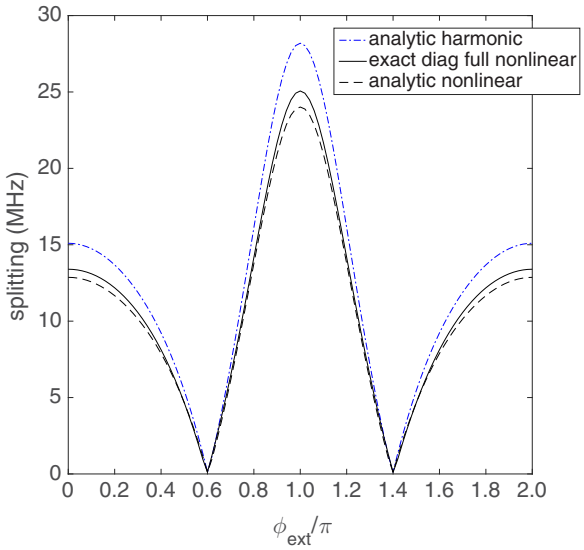

FIG. 3. (Color online) Splitting (equal to twice the magnitude of the coupling) in the fully nonlinear model (18) calculated by exact diagonalization (solid curve). Also shown are the corresponding harmonic approximation (dashed-dotted curve) and perturbative nonlinear (dashed) results.

$$|\varphi_1,\varphi_2\rangle \ \text{ with } \ \varphi_i \in \{-\pi, -\pi + d\varphi, \ldots, 0, \ldots, \pi\}, \tag{19}$$

where $d\varphi$ is the mesh spacing. The kinetic energy operator for coordinate φ_1 is approximated as

$$\text{KE}_1\,|\varphi_1,\varphi_2\rangle = -\frac{\hbar^2}{2C_1(\Phi_0/2\pi)^2\,d\phi^2} \times (|\varphi_1+d\phi,\varphi_2\rangle + |\varphi_1-d\phi,\varphi_2\rangle), \tag{20}$$

and similarly for that of φ_2. This tight-binding approximation replaces the quadratic kinetic energy in (18) by a cosine with the same curvature. We note that the factor of $\hbar^2$ in the numerator of (20) is required because the p_i in (18) are dimensionless. The potential energy is diagonal in the basis (19), and for each $|\varphi_1,\varphi_2\rangle$ is found by numerically minimizing the potential (15) with respect to the two massless variables ξ_1 and ξ_2. The exact diagonalization result is shown in the solid curve in Fig. 3 along with that of the harmonic approximation $2|g|$ and the perturbative result of Sec. V.

V. PERTURBATIVE TREATMENT OF NONLINEARITY

In this section we show that the form and strength of the qubit-qubit coupling can be derived analytically by treating the nonlinearity in (15) perturbatively. First we expand (15) in powers of the deviations φ_i and ξ_i, keeping all terms to quartic

order. This leads to

$$U = \sum_{i=1,2}\left\{\left(\frac{\Phi_0}{2\pi}\right)^2\left[\frac{\xi_i^2}{2L_{0i}} + \frac{(\varphi_i-\xi_i)^2}{2L_{ji}} - \lambda\frac{(\varphi_i-\xi_i)^4}{24L_{ji}}\right]\right\} + \left(\frac{\Phi_0}{2\pi}\right)^2\left[\cos(\delta)\,\frac{(\xi_1-\xi_2)^2}{2L_T} + \lambda'\sin(\delta)\,\frac{(\xi_1-\xi_2)^3}{6L_T} - \lambda'\cos(\delta)\,\frac{(\xi_1-\xi_2)^4}{24L_T}\right] + \text{const.}, \tag{21}$$

where parameters $\lambda = 1$ and $\lambda' = 1$ have been introduced to track powers of the qubit and coupler junction nonlinearities, respectively. Note that the first-order terms vanish on account of conditions (7) and (8), and that the coupler junction induces both cubic and quartic nonlinearity. In this section we develop a theory of the coupling to first order in λ and λ', neglecting all second-order corrections, including those of order $\lambda\lambda'$.

Because there is no kinetic energy associated with the massless ξ_i coordinates, we can eliminate them from the Hamiltonian by replacing $U(\varphi_1,\varphi_2,\xi_1,\xi_2)$ with $U(\varphi_1,\varphi_2,\xi_1^*,\xi_2^*)$, where the ξ_i^* minimize (21) for fixed φ_i. This procedure is different that what we did above in (7) and (8), because there we minimized U with respect to all four coordinates. Differentiation of (21) with respect to the ξ_i leads to a pair of equations that can be written as

$$\frac{\xi_1^*}{L_{\Sigma1}} - \cos(\delta)\frac{\xi_2^*}{L_T} = \frac{\varphi_1}{L_{j1}} - \lambda\frac{(\varphi_1-\xi_1^*)^3}{6L_{j1}} - \lambda'\sin(\delta)\frac{(\xi_1^*-\xi_2^*)^2}{2L_T} + \lambda'\cos(\delta)\frac{(\xi_1^*-\xi_2^*)^3}{6L_T} \tag{22}$$

and

$$\frac{\xi_2^*}{L_{\Sigma2}} - \cos(\delta)\,\frac{\xi_1^*}{L_T} = \frac{\varphi_2}{L_{j2}} - \lambda\frac{(\varphi_2-\xi_2^*)^3}{6L_{j2}} + \lambda'\sin(\delta)\frac{(\xi_1^*-\xi_2^*)^2}{2L_T} - \lambda'\cos(\delta)\frac{(\xi_1^*-\xi_2^*)^3}{6L_T}, \tag{23}$$

where

$$\frac{1}{L_{\Sigma i}} \equiv \frac{1}{L_{ji}} + \frac{1}{L_{0i}} + \frac{\cos(\delta)}{L_T}. \tag{24}$$

We solve the coupled nonlinear equations (22) and (23) perturbatively, to first order in λ and λ', by expanding

$$\xi_i^* = \xi_i^{(0)} + \xi_i^{(1)}, \quad (i = 1,2) \tag{25}$$

where the $\xi_i^{(0)}$ are zeroth order in the nonlinearity and the $\xi_i^{(1)}$ are first order. The zeroth order solutions are

$$\xi_i^{(0)} = \alpha_i\varphi_i + \beta_{\bar{i}}\varphi_{\bar{i}}, \tag{26}$$

where

$$\alpha_i \equiv \frac{1}{L_{ji}L_{\Sigma\bar{i}}D}, \quad \beta_i \equiv \frac{\cos(\delta)}{L_{ji}L_TD}, \tag{27}$$

and where $\bar{i}$ is the index complement to i:

$$\bar{1} = 2 \quad \text{and} \quad \bar{2} = 1. \tag{28}$$

Here

$$D \equiv \frac{1}{L_{\Sigma1}L_{\Sigma2}} - \frac{\cos^2(\delta)}{L_T^2}. \tag{29}$$

The first-order corrections are

$$\xi_1^{(1)} = -\frac{\lambda}{6}\left[\alpha_1\left(\varphi_1-\xi_1^{(0)}\right)^3 + \beta_2\left(\varphi_2-\xi_2^{(0)}\right)^3\right] + \lambda'\frac{A}{D}\left[\frac{1}{L_{\Sigma2}} - \frac{\cos(\delta)}{L_T}\right],$$
$$\xi_2^{(1)} = -\frac{\lambda}{6}\left[\alpha_2\left(\varphi_2-\xi_2^{(0)}\right)^3 + \beta_1\left(\varphi_1-\xi_1^{(0)}\right)^3\right] - \lambda'\frac{A}{D}\left[\frac{1}{L_{\Sigma1}} - \frac{\cos(\delta)}{L_T}\right], \tag{30}$$

where

$$A \equiv -\frac{\sin(\delta)}{2L_T}[(\alpha_1-\beta_1)\varphi_1 - (\alpha_2-\beta_2)\varphi_2]^2 + \frac{\cos(\delta)}{6L_T}[(\alpha_1-\beta_1)\varphi_1 - (\alpha_2-\beta_2)\varphi_2]^3. \tag{31}$$

Using (26) and (30) we obtain

$$H = \sum_{i=1,2}\left(\frac{2\pi}{\Phi_0}\right)^2\frac{p_i^2}{2C_i} + U^{(0)} + U^{(1)}, \tag{32}$$

where

$$U^{(0)} = \sum_{i=1,2}\left(\frac{\Phi_0}{2\pi}\right)^2\frac{\varphi_i^2}{2L_{qi}} + \left(\frac{\Phi_0}{2\pi}\right)^2\Gamma_{11}\,\varphi_1\varphi_2, \tag{33}$$

$$\frac{1}{L_{qi}} \equiv \frac{(1-\alpha_i)^2}{L_{ji}} + \frac{\alpha_i^2}{L_{0i}} + \frac{\beta_i^2}{L_{j\bar{i}}} + \frac{\beta_i^2}{L_{0\bar{i}}} + \cos(\delta)\,\frac{(\alpha_i-\beta_i)^2}{L_T}, \tag{34}$$

$$\Gamma_{11} \equiv \frac{(\alpha_1-1)\beta_2}{L_{j1}} + \frac{(\alpha_2-1)\beta_1}{L_{j2}} + \frac{\alpha_1\beta_2}{L_{01}} + \frac{\alpha_2\beta_1}{L_{02}} - \cos(\delta)\,\frac{(\alpha_1-\beta_1)(\alpha_2-\beta_2)}{L_T}, \tag{35}$$

and where

$$U^{(1)} = \left(\frac{\Phi_0}{2\pi}\right)^2\left\{\sum_{i=1,2}\left[\frac{\xi_i^{(0)}\xi_i^{(1)}}{L_{0i}} + \frac{\left(\xi_i^{(0)}-\varphi_i\right)\xi_i^{(1)}}{L_{ji}} - \lambda\frac{\left(\xi_i^{(0)}-\varphi_i\right)^4}{24\,L_{ji}}\right] + \cos(\delta)\,\frac{\left(\xi_1^{(0)}-\xi_2^{(0)}\right)\left(\xi_1^{(1)}-\xi_2^{(1)}\right)}{L_T} + \lambda'\sin(\delta)\,\frac{\left(\xi_1^{(0)}-\xi_2^{(0)}\right)^3}{6L_T} - \lambda'\cos(\delta)\,\frac{\left(\xi_1^{(0)}-\xi_2^{(0)}\right)^4}{24L_T}\right\} \tag{36}$$

is the anharmonic correction.

A. Coupling in the linearized model

The Hamiltonian in the harmonic approximation is

$$H = \sum_i H_i + \delta H, \tag{37}$$

where [see (32)]

$$H_i \equiv \left(\frac{2\pi}{\Phi_0}\right)^2\frac{p_i^2}{2C_i} + \left(\frac{\Phi_0}{2\pi}\right)^2\frac{\varphi_i^2}{2L_{qi}}, \quad (i = 1,2) \tag{38}$$

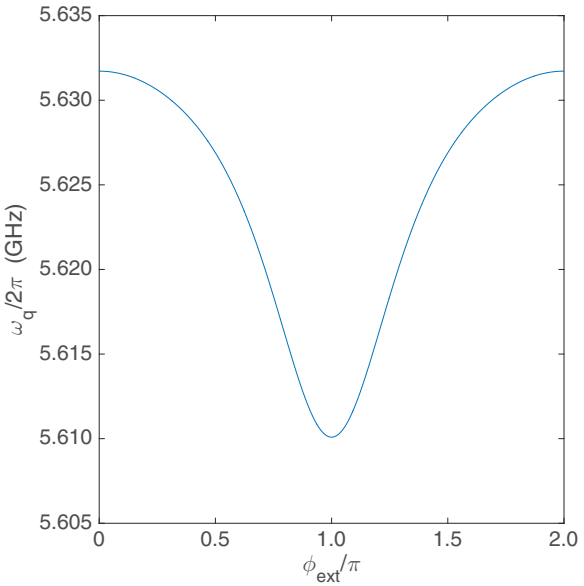

FIG. 4. (Color online) Qubit frequency (40) as a function of external flux, assuming circuit parameters of Table I. We see that $\omega_q/2\pi$ varies by about 22 MHz in this example.

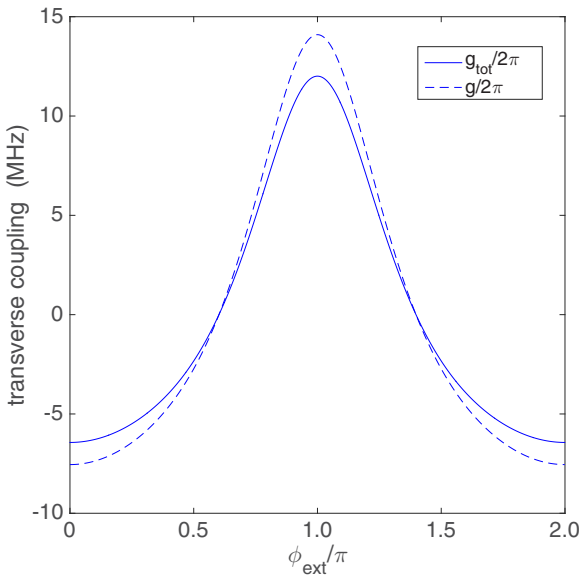

FIG. 5. (Color online) Coupling strength in the perturbative nonlinear approximation for system parameters given in Table I. The dashed line is coupling (44) in the linearized model.

and

$$\delta H \equiv \left(\frac{\Phi_0}{2\pi}\right)^2 \Gamma_{11}\,\varphi_1\varphi_2. \tag{39}$$

The Hamiltonian (38) describes a harmonic oscillator with flux-dependent frequency

$$\omega_{qi} \equiv \sqrt{\frac{1}{L_{qi}C_i}}, \tag{40}$$

which is plotted in Fig. 4 for the parameters of Table I.

In Appendix A we calculate the transverse coupling g resulting from a $\varphi_1\varphi_2$ interaction between a pair of identical classical harmonic oscillators. Here we derive the same result quantum mechanically (and for nonidentical qubits). Let $|0\rangle_i$ and $|1\rangle_i$ be the ground and first excited state of H_i (these are different than the eigenstates of the uncoupled qubits and they depend on ϕ_{ext}). Now we project the interaction term (39) into this basis. Each Josephson phase operator projects according to

$$\begin{aligned}\varphi &\to \begin{pmatrix}\varphi_{00} & \varphi_{01}\\ \varphi_{10} & \varphi_{11}\end{pmatrix}\\ &= \varphi_{01}\,\sigma^x - \left(\frac{\varphi_{11}-\varphi_{00}}{2}\right)\sigma^z + \left(\frac{\varphi_{00}+\varphi_{11}}{2}\right) I,\end{aligned} \tag{41}$$

where $\varphi_{mm'} \equiv \langle m|\varphi|m'\rangle$. By symmetry $\varphi_{00} = \varphi_{11} = 0$, and because the potential in (38) is parabolic,

$$\varphi_{01} = \left(\frac{2\pi}{\Phi_0}\right)\sqrt{\frac{\hbar L_q\,\omega_q}{2}}. \tag{42}$$

Then we obtain, from (39),

$$\delta H = g\,\sigma_1^x\sigma_2^x, \tag{43}$$

where

$$g = \frac{\hbar\Gamma_{11}\sqrt{L_{q1}L_{q2}}}{2}\sqrt{\omega_{q1}\omega_{q2}}. \tag{44}$$

The coupling strength (44) is generally different than the simpler weak-coupling expression (4). However for the system parameters of Table I they differ by no more than about 0.1 MHz.

B. Nonlinear correction to transverse coupling

To evaluate (36) we will express (30) in terms of the coordinates φ_1 and φ_2. We note from (30) and (36) that qubit nonlinearity λ generates quartic terms in the corrections to the potential energy, whereas the coupler nonlinearity λ' generates both cubic and quartic terms. Although the complete expressions for $\xi_1^{(1)}$ and $\xi_2^{(1)}$ in terms of the φ_i are quite complicated, they simplify when the circuit elements have identical parameters that satisfy

$$L_0 \ll L_j \ll L_T. \tag{45}$$

The nonlinear correction to the transverse coupling in the limit (45) is calculated in Appendix B.

The total transverse coupling

$$g_{tot} \equiv g + \delta g \tag{46}$$

obtained from (44) and (B18) is plotted in Fig. 5. Note that nonlinear contribution zeros precisely where the linear coupling does, and that the correction always suppresses the magnitude of the coupling. The amount of coupling suppression can be simply quantified by writing (46) as

$$g_{tot} = \zeta\, g, \quad \text{where} \quad \zeta \equiv 1 + \frac{\delta g}{g}. \tag{47}$$

We emphasize that g in (47) refers to the coupling (4) or (44) for the linearized circuit. To estimate ζ we again assume (45),

which leads to

$$\zeta \approx 1 - \pi^2 \left(\frac{\hbar \omega_q}{\Phi_0^2 / 2 L_j} \right) = 0.852, \tag{48}$$

using a qubit frequency of 5.62 GHz and the value of L_j from Table I. Therefore we find that qubit nonlinearity suppresses the transverse coupling by about 15%, and that the effects of coupler nonlinearity (corrections proportional to λ') are negligible in the parameter regime considered.

To validate the perturbative corrections we compare, in Fig. 3, the splitting $2|g_{tot}|$ between the symmetric and antisymmetric eigenstates to the fully nonlinear result obtained by exact diagonalization. We find that the analytic approximation developed here is in very good agreement with the numerical results. It can be shown that the small differences arise not from the replacement of the cosine potentials by their quadratic plus quartic expansions, but from (i) keeping only the terms first order in λ and λ' in the subsequent analysis, and (ii) assuming the limit (45).

VI. DIAGONAL COUPLING

The coupler circuit of Fig. 1 also produces a small diagonal qubit-qubit interaction of the form

$$\delta H = J \sigma_1^z \sigma_2^z. \tag{49}$$

In this section we calculate J, analytically and numerically, by relating it to the exact eigenstates of the coupled qubit system [20],

$$J = \frac{E_{11} - (E_+ + E_-) + E_{00}}{4}, \tag{50}$$

and throughout this section we assume resonantly tuned qubits. Here E_{11} is the energy of the $|11\rangle$ state,

$$E_\pm = \omega_q \pm |g| + E_{00} \tag{51}$$

are the energies of the single-excitation eigenstates, with ω_q the frequency of the uncoupled qubits, and E_{00} is the ground-state energy. Note that J is to be computed in the presence of the total transverse interaction

$$\delta H = g \, \sigma_1^x \sigma_2^x, \tag{52}$$

where in this section we write g_{tot} [defined in (46)] simply as g.

Two types of effects contribute to the total diagonal coupling J. The dominant mechanism comes from states outside of the qubit subspace and is caused by the repulsion of $|11\rangle$ by the $|02\rangle$ and $|20\rangle$ eigenstates. These states differ in energy by the qubit anharmonicity

$$\eta \equiv (E_1 - E_0) - (E_2 - E_1). \tag{53}$$

Referring to the nonlinear Hamiltonian (B9), this contribution to J results from the terms proportional to Γ_{04} and Γ_{03}, which generate qubit anharmonicity, in the presence of a transverse interaction.

We can estimate this effect by considering the second-order correction to the energy of the $|11\rangle$ state resulting from the transverse interaction, which is

$$\delta E_{11} \approx 2 \times \frac{(\sqrt{2} g)^2}{\eta}, \tag{54}$$

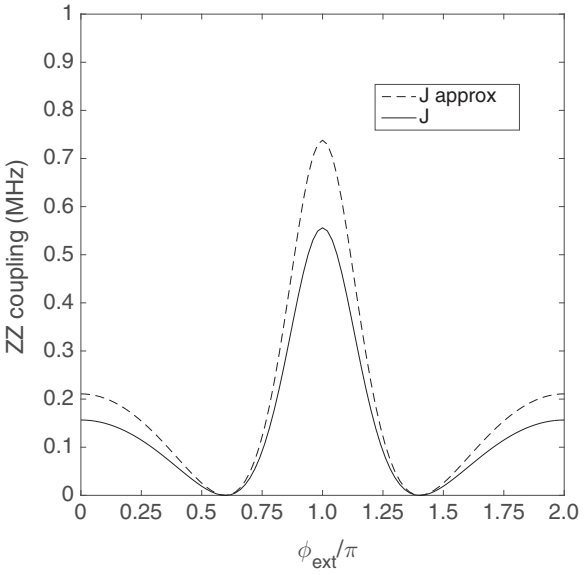

FIG. 6. Diagonal coupling strength (50) computed by exact diagonalization, and the approximation (55).

assuming harmonic oscillator eigenfunctions. The factor of 2 in (54) comes from the contributions by both $|02\rangle$ and $|20\rangle$. Then the $\sigma^z \otimes \sigma^z$ coupling strength is simply

$$J \approx \frac{g^2}{\eta}. \tag{55}$$

A few remarks about (55) are in order: The diagonal coupling resulting from the $|2\rangle$ state repulsion effect is always positive, and it zeros when the transverse coupling does. However, other contributions to J (see below) can have either sign. Also, the use of harmonic oscillator eigenfunctions will slightly overestimate the E_{11} repulsion and hence J. Finally, the anharmonicity and size of η generated by the terms proportional to Γ_{04} (which are dominant and flux independent) and Γ_{03} (which depends on Φ_{ext}) is an approximation, so in (55) we instead prefer to use an exactly calculated (or measured) value, which is approximately 213 MHz for uncoupled qubits with parameters of Table I.

The $\sigma^z \otimes \sigma^z$ coupling strength (50) for a system with parameters of Table I is shown in Fig. 6, along with the approximation (55). Here (50) is computed by exact diagonalization and is shown in the solid curve. The approximation (55) is evaluated by using the exact diagonalization result for the total transverse coupling g, with $\eta/2\pi = 213$ MHz, and is shown in the dashed curve. Although the approximation (55) necessarily zeros when g does, the exact value calculated from (50) does not have to. We find that the $\sigma^z \otimes \sigma^z$ coupling strength (50) calculated by exact diagonalization does reach a negative value of -110 Hz, but this tiny value may not be reliable given our numerical accuracy.

The second type of effects contributing to J result from the interaction terms proportional to Γ_{13}, Γ_{12}, and Γ_{22} in (B9). The Γ_{22} terms make the largest contribution to J, because they are the only ones that survive when the small anharmonic corrections to the qubit eigenfunctions are neglected. To estimate the Γ_{22} contributions we project the φ_i^2 operators

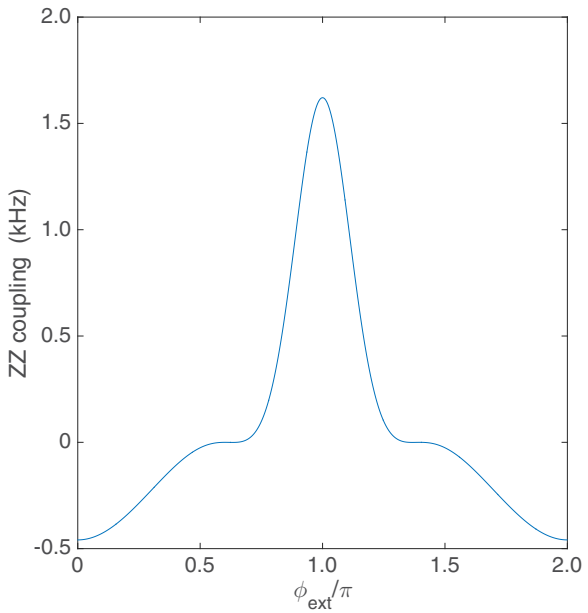

FIG. 7. (Color online) Subdominant contribution (57) to the diagonal coupling J, versus flux. This contribution zeros when g does.

as

$$\varphi^2 \to \begin{pmatrix} \langle 0|\varphi^2|0\rangle & \langle 0|\varphi^2|1\rangle \\ \langle 1|\varphi^2|0\rangle & \langle 1|\varphi^2|1\rangle \end{pmatrix} \approx \left(\frac{2\pi}{\Phi_0}\right)\hbar\omega_q L_q \times \left(I - \frac{1}{2}\sigma^z\right), \tag{56}$$

where I is the identity matrix and in the second step we have assumed harmonic eigenfunctions. This leads to an additional contribution

$$J = \Gamma_{22}\left(\frac{2\pi}{\Phi_0}\right)^2\left(\frac{\hbar\omega_q L_q}{2}\right)^2, \tag{57}$$

which is always much smaller than (55) and also zeros when g does. The subdominant contribution (57) is plotted in Fig. 7 using the parameters of Table I.

VII. CONCLUSIONS

In this paper we have provided a detailed theoretical analysis of a tunable coupler design recently demonstrated for superconducting Xmon qubits [26]. Treating the leading-order nonlinear effects perturbatively, we find that the qubit nonlinearity significantly suppresses the magnitude of the transverse $\sigma^x \otimes \sigma^x$ coupling. Although an accurate evaluation of the size of this suppression requires the analysis provided in Secs. III and VI, a simple estimate follows if we assume the circuit parameters to satisfy the conditions (45). In this case, the suppression fraction is simply given by $2\pi^2\hbar\omega_q L_j/\Phi_0^2$.

In contrast to the qubit nonlinearity, the effects of coupler junction nonlinearity are found to be entirely negligible. This is because the coupler wires are connected to the qubits at low voltage nodes and the energy stored in the coupler junction is always small.

Finally, we comment on our choice of parameters given in Table I, and the behavior of the coupler as these values are varied. First, the qubit capacitances and inductances, C_i and L_{ji}, are largely determined by the target qubit frequency and the transmon condition that the charge noise be suppressed, so these parameters cannot be strongly varied in practice. However the L_{0i} and L_T parameters can be varied considerably. Although the results in this paper will apply in those cases as well, the coupler function $g(\phi_{ext})$ changes significantly. For example, suppose we wish to maximize the magnitude of the "on" coupling strength, which occurs when $\phi_{ext} = \pi$. In the harmonic approximation,

$$\max g = \frac{L_0^2}{2(L_j + L_0)(L_T - 2L_0)}\,\omega_q. \tag{58}$$

We can increase (58) by increasing L_0 and/or decreasing L_T, but only to a point, because of the pole at $L_T = 2L_0$. This pole results from the approximations used to obtain (4) and is of course unphysical: As $L_T \to 2L_0$, the nonlinear corrections to (4) become stronger, resulting in a finite maximum coupling of about 700 MHz, assuming $L_T = 2L_0$ and the other qubit parameters as in Table I.

However, in the present design, varying either L_0 or L_T increases the maximum coupling at the expense of shifting the entire coupling curve upward, thereby eliminating the regions of negative g. (For applications where negative values of coupling are not required, this is not an important restriction.) In addition, the coupling curve somewhat sharpens upon increasing L_0 and/or decreasing L_T, making experimental control more challenging. The values given in Table I are chosen to provide a reasonable maximum coupling strength combined with large negative coupling values and an experimentally convenient $g(\phi_{ext})$ profile.

ACKNOWLEDGMENTS

This research was funded by the US Office of the Director of National Intelligence (ODNI), Intelligence Advanced Research Projects Activity (IARPA), through the US Army Research Office Grant No. W911NF-10-1-0334. All statements of fact, opinion, or conclusions contained herein are those of the authors and should not be construed as representing the official views or policies of IARPA, the ODNI, or the US Government. This work was also supported by the US National Science Foundation under CDI Grant No. DMR-1029764. We thank Alexander Korotkov for useful discussions.

APPENDIX A: COUPLING IN THE HARMONIC LIMIT

The expression (4) can be derived, essentially classically, from the input impedances to the network of Fig. 8, defined through the relation

$$\begin{pmatrix} V_1 \\ V_2 \end{pmatrix} = \begin{pmatrix} L_q & M \\ M & L_q \end{pmatrix}\begin{pmatrix} \dot{I}_1 \\ \dot{I}_2 \end{pmatrix}. \tag{A1}$$

We find

$$M = \frac{L_0^2}{L_{eff} + 2L_0} \quad \text{and} \quad L_q = L_j + L_0 - M. \tag{A2}$$

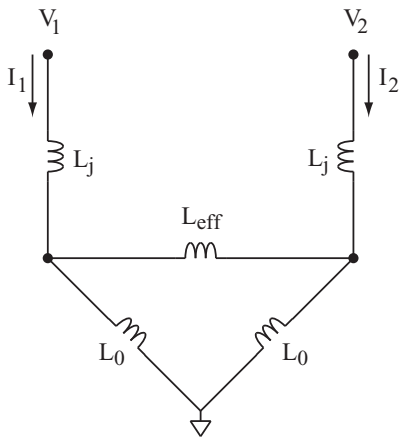

FIG. 8. Network of linear inductors.

The potential energy of the circuit in Fig. 1 in the harmonic approximation is therefore

$$U = \left(\frac{\Phi_0}{2\pi}\right)^2\left[\frac{\varphi_1^2}{2KL_q} + \frac{\varphi_2^2}{2KL_q} + \Gamma_{11}\varphi_1\varphi_2\right], \tag{A3}$$

where

$$K = 1 - \left(\frac{M}{L_q}\right)^2 \quad \text{and} \quad \Gamma_{11} = -\frac{M}{KL_q^2}. \tag{A4}$$

In the weakly coupled limit, $M \ll L_q$. To obtain (4) we assume

$$K \approx 1, \tag{A5}$$

$$L_q \approx L_j + L_0, \tag{A6}$$

and

$$\Gamma_{11} \approx -\frac{L_0^2}{(L_j + L_0)^2(L_{\text{eff}} + 2L_0)}. \tag{A7}$$

These approximations are removed in Sec. V.

Next we calculate the splitting induced by (A7). We can again compute this classically by treating the qubits as LC oscillators with frequency $\omega_q = (L_qC)^{-\frac{1}{2}}$, where L_q is given by (A6). The potential energy of the coupled oscillators is given in (A3) with $K = 1$. Diagonalizing the quadratic form (A3) leads to eigenmodes with shifted inductances $1/(L_q^{-1} \pm \Gamma_{11})$ and hence frequencies $\sqrt{1 \pm L_q\Gamma_{11}}\,\omega_q$. Therefore in the weakly coupled limit we obtain

$$g = \frac{\Gamma_{11}L_q}{2}\,\omega_q, \tag{A8}$$

a result that also applies to coupled qubits and leads to the expression (4).

APPENDIX B: NONLINEAR CORRECTIONS

In limit (45) we have

$$L_q \to L_j, \tag{B1}$$

$$L_\Sigma \to L_0, \tag{B2}$$

$$D \to \frac{1}{L_0^2}, \tag{B3}$$

$$\alpha \to \frac{L_0}{L_j}, \tag{B4}$$

$$\beta \to \frac{\cos(\delta)\,L_0^2}{L_jL_T}, \tag{B5}$$

and therefore

$$\beta \ll \alpha \ll 1. \tag{B6}$$

In this section we derive analytic expressions for the nonlinear corrections assuming (45), which is a special case of the weak coupling assumption of Sec. I. Using (B6) we find that

$$\xi_1^{(1)} \approx \lambda\left(-\frac{\alpha}{6}\varphi_1^3 + \frac{\alpha\beta}{2}\varphi_1^2\varphi_2 + \frac{\beta^2}{2}\varphi_1\varphi_2^2 - \frac{\beta}{6}\varphi_2^3\right) - \lambda'\frac{\alpha^2L_0\sin\delta}{2L_T}\left(\varphi_1^2 - \varphi_1\varphi_2 + \varphi_2^2\right) \tag{B7}$$

and

$$\xi_2^{(1)} \approx \lambda\left(-\frac{\alpha}{6}\varphi_2^3 + \frac{\alpha\beta}{2}\varphi_1\varphi_2^2 + \frac{\beta^2}{2}\varphi_1^2\varphi_2 - \frac{\beta}{6}\varphi_1^3\right) + \lambda'\frac{\alpha^2L_0\sin\delta}{2L_T}\left(\varphi_1^2 - \varphi_1\varphi_2 + \varphi_2^2\right). \tag{B8}$$

These expressions are obtained by considering every term allowed by symmetry and approximating its coefficient by that of the dominant contribution (using $\lambda = \lambda' = 1$). The correction (36) is similarly obtained by assuming identical qubits and finding the largest contribution to every possible term in the energy. The result is

$$U^{(1)} = \left(\frac{\Phi_0}{2\pi}\right)^2\left[\lambda\,\Gamma_{04}\left(\varphi_1^4 + \varphi_2^4\right) + \lambda'\Gamma_{03}\left(\varphi_1^3 - \varphi_2^3\right) + \lambda\,\Gamma_{13}\left(\varphi_1\varphi_2^3 + \varphi_1^3\varphi_2\right) + \lambda'\Gamma_{12}\left(\varphi_1\varphi_2^2 - \varphi_1^2\varphi_2\right) + \lambda\Gamma_{22}\varphi_1^2\varphi_2^2\right], \tag{B9}$$

where

$$\Gamma_{04} = -\frac{1}{24L_j}, \tag{B10}$$

$$\Gamma_{03} = \frac{\alpha^3\sin\delta}{6L_T}, \tag{B11}$$

$$\Gamma_{13} = \frac{\alpha^2\cos\delta}{6L_T}, \tag{B12}$$

$$\Gamma_{12} = \frac{\alpha^3\sin\delta}{2L_T}, \tag{B13}$$

$$\Gamma_{22} = \alpha\beta\left(\frac{\beta}{L_0} - \frac{\alpha\cos\delta}{L_T}\right). \tag{B14}$$

The dominant nonlinear correction to the transverse coupling is

$$\delta g = \left(\frac{\Phi_0}{2\pi}\right)^2\Gamma_{13}\,\langle 01|\varphi_1\varphi_2^3 + \varphi_1^3\varphi_2|10\rangle. \tag{B15}$$

To evaluate (B15) note that $\langle 01|\varphi_1\varphi_2^3 + \varphi_1^3\varphi_2|10\rangle = 2\varphi_{01}\langle 0|\varphi^3|1\rangle$, where φ_{01} is defined in (42) and

$$\langle 0|\varphi^3|1\rangle = 3\left(\frac{2\pi}{\Phi_0}\right)^3\left(\frac{\hbar L_q\,\omega_q}{2}\right)^{\frac{3}{2}}. \tag{B16}$$

Then (B15) can be written as

$$\delta g = \frac{3}{2}\,\Gamma_{13}\left(\frac{\hbar\omega_q L_q}{\Phi_0/2\pi}\right)^2 \tag{B17}$$

$$= \cos(\delta)\frac{\pi^2\alpha^2 L_j}{2L_T}\left(\frac{\hbar\omega_q}{\Phi_0^2/2L_j}\right)\hbar\omega_q. \tag{B18}$$

[1] J. Koch, T. M. Yu, J. Gambetta, A. A. Houck, D. I. Schuster, J. Majer, A. Blais, M. H. Devoret, S. M. Girvin, and R. J. Schoelkopf, Phys. Rev. A **76**, 042319 (2007).

[2] R. Barends, J. Kelly, A. Megrant, D. Sank, E. Jeffrey, Y. Chen, Y. Yin, B. Chiaro, J. Mutus, C. Neill, P. O'Malley, P. Roushan, J. Wenner, T. C. White, A. N. Cleland, and J. M. Martinis, Phys. Rev. Lett. **111**, 080502 (2013).

[3] R. Barends, J. Kelly, A. Megrant, A. Veitia, D. Sank, E. Jeffrey, T. C. White, J. Mutus, A. G. Fowler, B. Campbell, Y. Chen, Z. Chen, B. Chiaro, A. Dunsworth, C. Neill, P. O'Malley, P. Roushan, A. Vainsencher, J. Wenner, A. N. Korotkov, A. N. Cleland, and J. M. Martinis, Nature (London) **508**, 500 (2014).

[4] A. Mezzacapo, L. Lamata, S. Filipp, and E. Solano, Phys. Rev. Lett. **113**, 050501 (2014).

[5] D. Marcos, P. Widmer, E. Rico, M. Hafezi, P. Rabl, U.-J. Wiese, and P. Zoller, Ann. Phys. (NY) **351**, 634 (2014).

[6] M. R. Geller, J. M. Martinis, A. T. Sornborger, P. C. Stancil, E. J. Pritchett, H. You, and A. Galiautdinov, Phys. Rev. A **91**, 062309 (2015).

[7] Y. Makhlin, G. Schön, and A. Shnirman, Nature (London) **398**, 305 (1999).

[8] A. Blais, A. Maassen van den Brink, and A. M. Zagoskin, Phys. Rev. Lett. **90**, 127901 (2003).

[9] B. L. T. Plourde, J. Zhang, K. B. Whaley, F. K. Wilhelm, T. L. Robertson, T. Hime, S. Linzen, P. A. Reichardt, C.-E. Wu, and J. Clarke, Phys. Rev. B **70**, 140501(R) (2004).

[10] J. Lantz, M. Wallquist, V. S. Shumeiko, and G. Wendin, Phys. Rev. B **70**, 140507 (2004).

[11] M. Grajcar, Y.-X. Liu, F. Nori, and A. M. Zagoskin, Phys. Rev. B **74**, 172505 (2006).

[12] T. Hime, P. A. Reichardt, B. L. T. Plourde, T. L. Robertson, C.-E. Wu, V. A. Ustinov, and J. Clarke, Science **314**, 1427 (2006).

[13] S. H. W. van der Ploeg, A. Izmalkov, A. M. van den Brink, U. Hubner, M. Grajcar, E. Il'ichev, H.-G. Meyer, and A. M. Zagoskin, Phys. Rev. Lett. **98**, 057004 (2007).

[14] A. O. Niskanen, K. Harrabi, F. Yoshihara, Y. Nakamura, S. Lloyd, and J. S. Tsai, Science **316**, 723 (2007).

[15] R. Harris, A. J. Berkley, M. W. Johnson, P. Bunyk, S. Govorkov, M. C. Thom, S. Uchaikin, A. B. Wilson, J. Chung, E. Holtham, J. D. Biamonte, A. Y. Smirnov, M. H. S. Amin, and A. Maassen van den Brink, Phys. Rev. Lett. **98**, 177001 (2007).

[16] S. Ashhab, A. O. Niskanen, K. Harrabi, Y. Nakamura, T. Picot, P. C. de Groot, C. J. P. M. Harmans, J. E. Mooij, and F. Nori, Phys. Rev. B **77**, 014510 (2008).

[17] T. Yamamoto, M. Watanabe, J. Q. You, Y. A. Pashkin, O. Astafiev, Y. Nakamura, F. Nori, and J. S. Tsai, Phys. Rev. B **77**, 064505 (2008).

[18] M. Mariantoni, F. Deppe, A. Marx, R. Gross, F. K. Wilhelm, and E. Solano, Phys. Rev. B **78**, 104508 (2008).

[19] M. S. Allman, F. Altomare, J. D. Whittaker, K. Cicak, D. Li, A. Sirois, J. Strong, J. D. Teufel, and R. W. Simmonds, Phys. Rev. Lett. **104**, 177004 (2010).

[20] R. A. Pinto, A. N. Korotkov, M. R. Geller, V. S. Shumeiko, and J. M. Martinis, Phys. Rev. B **82**, 104522 (2010).

[21] J. M. Gambetta, A. A. Houck, and A. Blais, Phys. Rev. Lett. **106**, 030502 (2011).

[22] R. C. Bialczak, M. Ansmann, M. Hofheinz, M. Lenander, E. Lucero, M. Neeley, A. D. O'Connell, D. Sank, H. Wang, M. Weides, J. Wenner, T. Yamamoto, A. N. Cleland, and J. M. Martinis, Phys. Rev. Lett. **106**, 060501 (2011).

[23] S. J. Srinivasan, A. J. Hoffman, J. M. Gambetta, and A. A. Houck, Phys. Rev. Lett. **106**, 083601 (2011).

[24] P. Groszkowski, A. G. Fowler, F. Motzoi, and F. K. Wilhelm, Phys. Rev. B **84**, 144516 (2011).

[25] A. J. Hoffman, S. J. Srinivasan, J. M. Gambetta, and A. A. Houck, Phys. Rev. B **84**, 184515 (2011).

[26] Y. Chen, C. Neill, P. Roushan, N. Leung, M. Fang, R. Barends, J. Kelly, B. Campbell, Z. Chen, B. Chiaro, A. Dunsworth, E. Jeffrey, A. Megrant, J. Y. Mutus, P. J. J. O'Malley, C. M. Quintana, D. Sank, A. Vainsencher, J. Wenner, T. C. White, M. R. Geller, A. N. Cleland, and J. M. Martinis, Phys. Rev. Lett. **113**, 220502 (2014).